European Journal of Medicinal Chemistry 48 (2012) 391–401

Contents lists available at SciVerse ScienceDirect

European Journal of Medicinal Chemistry

journal homepage: http://www.elsevier.com/locate/ejmech

Short communication

Design, synthesis and biological evaluation of pyrazole derivatives as potential multi-kinase inhibitors in hepatocellular carcinoma

Elena Strocchi [a], Francesca Fornari [b], Manuela Minguzzi [b], Laura Gramantieri [b], Maddalena Milazzo [b], Valentina Rebuttini [a], Simone Breviglieri [a], Carlo Maurizio Camaggi [a], Erica Locatelli [a], Luigi Bolondi [b], Mauro Comes-Franchini [a,*]

[a] Department of Organic Chemistry "A. Mangini", University of Bologna, Viale Risorgimento 4, 40136 Bologna, Italy
[b] Department of Clinical Medicine and Center for Applied Biomedical Research, S. Orsola-Malpighi Universitary Hospital, University of Bologna, Via Massarenti 9, 40138 Bologna, Italy

ARTICLE INFO

Article history:
Received 24 May 2011
Received in revised form
7 October 2011
Accepted 20 December 2011
Available online 29 December 2011

Keywords:
Pyrazole
Dipolar cycloaddition
Hepatocellular carcinoma
Molecular docking
Kinase inhibitors

ABSTRACT

We described the optimization, by molecular modelling, of small pyrazole derivatives, as kinase inhibitors, obtained through a 1,3-dipolar cycloaddition between nitrile imines and functionalized acetylenes. The two compounds, selected as potential agents active against hepatocellular carcinoma (HCC) were then evaluated *in vitro* for their biological activity on HCC-derived cell lines. The compounds show a promising inhibitory growth efficacy (IC_{50} 50–100 μM) in SNU449 cell line, as well as block of cell cycle progression and induction of apoptosis, and can be considered as lead compounds for further SAR developments.

1. Introduction

Hepatocellular carcinoma (HCC) accounts for 80–90% of primary liver cancers and it is the third cause of death from cancer worldwide [1]. The high lethality of HCC is partly due to its resistance to traditional chemotherapics. Despite the survival advantage achieved by Sorafenib, effective treatments for advanced HCC are still needed [2]. It was recently reported that combination of specific AKT inhibitors with Sorafenib restored the sensitivity of resistant cells to apoptotic cell death [3].

In the recent years the involvement of different molecular alterations that arise during the development and progression of HCC have been reported [4]. In particular, aberrant activation of different cellular pathways such as IGF, Ras, PI3K/Akt/mTOR and Wnt signalling has been identified in HCC [5,6]. The serine/threonine kinase AKT acts as a regulator of important cellular processes, such as cell cycle, cell survival and cell growth. In HCC, over expression of this pathway is associated with poor prognosis [7], invasion and metastasis [8]. The binding of growth factors (e.g. IGF and EGF) to their receptors activates PI3K, which in turn activates the serine/threonine kinase AKT. It is reported that about 20% of HCC patients had elevated levels of AKT phosphorylation on Ser-473 [9]. Moreover, levels of phosphorylated mTOR and p70 S6 kinase resulted increased in 15% and 45% of HCC cases, respectively [10].

Recent evidences showed that inhibition of the PI3K/AKT/mTOR pathway with a Rapamacyn analogue, Everolimus, slowed tumour growth and increased survival in a HCC xenograft model, suggesting that the activation of this pathway exerts a crucial role in hepatocarcinogenesis [7].

In an attempt to search for novel antitumour compounds, we focused our attention to multi-kinase inhibitor molecules and we investigated their antiproliferative activity on HCC-derived cell lines.

Indeed, it has been reported that the 3,5-pyrazole ring is an interesting scaffold for the design of kinase inhibitors targeting the ATP pocket of protein kinases [11–14].

Owing to its high synthetic efficiency and high regio- and stereo selectivity, the 1,3-dipolar cycloaddition (1,3-DC) of 1,3-dipoles with π-electronic-deficient systems has emerged as a popular way for the obtainment of heterocycles [15]. In particular, nitrogen-containing heterocycles have attracted widespread attention in the field of synthetic organic chemistry as well as in medicinal chemistry [16]. Among them, pyrazoles are synthetic targets of utmost

* Corresponding author. Tel.: +390512093626; fax: +390512093654.
E-mail address: mauro.comesfranchini@unibo.it (M. Comes-Franchini).

0223-5234/$ – see front matter © 2011 Elsevier Masson SAS. All rights reserved.
doi:10.1016/j.ejmech.2011.12.031

importance in the pharmaceutically industry, since such a five-membered heterocyclic moieties bear the core structure of numerous drugs [17].

Two general methods are known for the synthesis of pyrazoles. The first method involves the standard reaction of hydrazines with 1,3-difunctional substrates such as 1,3-dicarbonyl compounds [18], ynones [19] or β-aminoacrolein [20]. In addition, the 1,3-dipolar cycloaddition (1,3-DC) between alkynes and nitrile imines provides a direct access to pyrazoles [21], but regioisomeric mixtures of pyrazoles are frequently obtained.

Following our interest in 1,3-DC [22] and in the synthesis of kinase inhibitors [23] we have recently developed a method for the region-controlled synthesis of pyrazoles based on the 1,3-DC of nitrile imines with a class of functionalized acetylenes as the propionamides [24].

2. Results and discussion

2.1. Preliminary molecular docking

Our approach towards the synthesis of substituted pyrazoles as multi-kinase inhibitors involved a computer-assisted strategy in the molecular design. Docking simulations were performed for lead optimization and to characterize the binding pose and affinity of putative lead candidates to the ATP binding site of several kinases involved in HCC pathways (AKT, PI3K, GSK-3β, CDK2, AurA, MAPK, EGFR, IGFR). 3,5-disubstituted pyrazoles were found to have the minimum requirements for tight binding at the ATP active site of the kinase domain. Therefore, we started from a preliminary docking evaluation of some pyrazole derivatives obtainable through 1,3-DC.

For the subsequent development, structures substituted in position 5 of the pyrazole moiety through a carboxamide group and with an aryl groups in position 3 were explored. We evaluated two series of compounds with starting structures containing a phenylamine group at position 1 (which could either improve the water solubility of inhibitors and form hydrogen-bonds within the ATP cleft), a carboxamide-R group at position 5 and at postion 3: (1) carboxyl group or (2) dimethylphenyl moiety. Subsequent derived structures were characterized as follow: (1) aminophenyl connected to carboxamide at position 5 of pyrazole and carboxamide-dimethylphenyl at position 3; (2) aminophenyl connected to carboxamide at position 5 and dimethylphenyl at position 3.

The selected target proteins for the docking evaluation of the proposed compounds were retrieved from the Protein Data Bank (http://www.rcsb.org/pdb/) and were: AKT2 (PDB ID: 2jdr), GSK-3β (PDB ID: 1pyx), PI3K (PDB ID: 2v4l), CDK2 (PDB ID: 2j9m), MAPK (PDB ID ID: 2pzy), IGFR (PDB ID: 2zm3), EGFR (PDB ID: 2rpg), AurA (PDB ID: 2x6d).

Binding modes and binding affinities of the evaluated compounds within the ATP binding site of all the selected kinases were calculated using the Autogrid 4.0 and Autodock 4.1 programs [25]. The ADT 1.6.1 package was used for visualization of the results (see experimental section for the preparation of the molecules, preparation of the target macromolecules and for the procedure of molecular docking).

2.2. Analysis of the binding mode

We analyzed the location and orientation of the evaluated compounds and the interactions into the binding site of the selected kinases above indicated. The predicted binding free energy (that includes intermolecular energy and torsional free energy) was used as the criterion for ranking. The conformation with the lowest ranking docked binding energy was considered to be the "best" docking result.

Satisfactory docking results were observed for the two compounds then indicated as **Target A** and **Target B**, having the following structures in Fig. 1.

Both compounds, nicely fitted inside the ATP site pocket of the examined kinases, as indicated from binding free energy reported in Table 1 and from analysis of ligand binding pose inside the ATP pocket sites.

Better docking results seem to be observed to AKT2 with both compounds; the best poses of **Target A** and **Target B** into AKT2 binding site had an estimated binding free energy [ΔG] of −9.99, and −9.65 kcal/mol respectively. Nevertheless, both compounds show similar results with all the examined kinases.

Target A, characterized by a C-5-carboxamide with an amino-phenyl substituent and a C-3-dimethylphenyl substituent, exhibits slight better values of binding free energies to AKT2, PI3K and CDK2 kinases (Table 1), while **Target B** shows better binding affinity to the remaining kinases.

The best poses, obtained after docking to different kinases PDB structures, suggest that the binding conformation of **Target A** is similar to that reported for **Target B** in all kinases, and that are typical of aspecific ATP competitors. The binding poses of **Target A** and **Target B** into ATP binding site of AKT2 and GSK-3β are shown in Fig. 2.

In all the cases, the substituted heterocyclic scaffold fitted and entered into the ATP binding site with good binding affinity.

Target B could form two or three hydrogen-bonds into the binding site of the selected kinases, showing interactions between the terminal aminogroup of phenylamines with a carboxyl of GLU (AKT2: GLU230 and Glu200) or ASP residues (GSK-3β: ASP133), and between carbonyl of C5-carboxamide and NH_3+ of LYS residue (GSK-3β: LYS85), or between NH of C5-carboxamide and OH of THR (AKT2: THR-292) respectively.

Target A could form two hydrogen-bonds into the binding site of the selected kinases, showing interactions between the terminal aminogroup of phenylamines with a carboxyl of GLU or ASP residues (AKT2: GLU200 and GLU230; GSK-3β: ASP133) or carbonyl in the backbones of PRO residues (GSK-3β: PRO136).

The examined compounds revealed a common binding mode in the hydrophobic cleft also through a complementary apolar interaction surface. Pyrazole ring or the hydrophobic aryl moieties fit tightly into the ATP binding site of the different kinases through pi–pi interactions with the aromatic ring of PHE or TYR residues.

Pi-cation interactions between the amino-substituted phenyl ring, connected through an amide linkage – to the pyrazole ring (in position 5) and the protonated aminogroup of LYS residues, are present for both compounds docked with the selected kinases.

The two above described structures, with more promising docking results, were therefore suggested for the synthesis and testing as multi-kinase inhibitors.

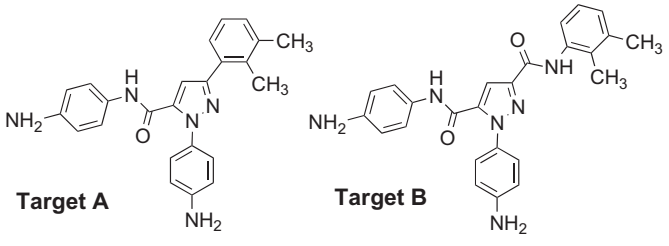

Fig. 1. Chemical structures for **Target A** and **Target B**.

Table 1
Docking results, expressed in term of binding free energy (Δ*G*, kcal/mol).

	Target kinases							
	AKT2	GSK-3β	PI3K	EGFR	IGFR	CDK2	AurA	MAPK
Target A	−9.99	−8.80	−9.33	−9.19	−8.24	−9.67	−8.49	−8.53
Target B	−9.65	−9.23	−8.99	−9.46	−8.24	−9.61	−8.84	−9.02

2.3. Synthesis

For the synthesis of tert-butyl (4-propiolamidophenyl)carbamate **1**, commercially available propiolic acid was reacted in diethyl ether with N-*p*-Boc-phenylendiamine in the presence of dicyclohexylcarbodiimide (DCC) and 4-dimethylaminopyridine (DMAP) in THF for 24 h giving **1** in 72% yield. (E)-2,3-dimethyl-N′-(4-nitrophenyl)benzohydrazonoyl chloride **2** and (Z)-methyl-2-(2-(4-((tert-butoxycarbonyl)amino)phenyl) hydrazono)-2-chloroacetate **3** have been prepared as already reported by us [23]. The *C*-aryl-*N*-aryl hydrazonoyl chloride **2** was obtained starting from the corresponding p-nitrophenyl hydrazines.

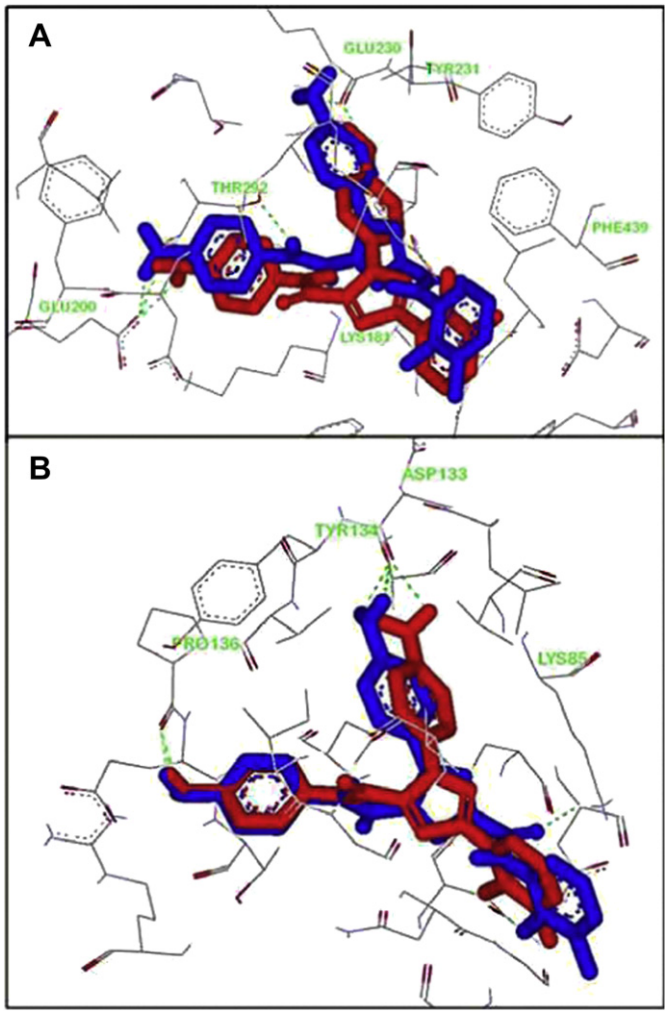

Fig. 2. The image display the low energy conformations of **Target A** and **Target B**. On the top (A): best docking binding poses of **Target A** (red) and **Target B** (blue) into the ATP binding site of AKT2. On the bottom (B): best docking binding poses of **Target A** (red) and **Target B** (blue) into binding site of GSK-3β. The aminoacidic residues of binding pockets closed to molecules and involved in H-bonds (shown in green), pi–pi and pi–cation interactions are indicated. (For interpretation of the references to colour in this figure legend, the reader is referred to the web version of this article.)

The reaction with 2,3-dimethylbenzoylchloride (obtained in quantitative yield from the carboxylic acid) in THF in the presence of Et_3N gave the corresponding benzoylhydrazine in 75% yield. The subsequent reaction of 2,3-dimethyl-*N*′-(4-nitrophenyl)benzohydrazide with triphenylphosphine-CCl_4 in CH_3CN [17] gave the hydrazonoyl chlorides **2** in 86% yield. The *C*-carboxymethyl-*N*-aryl hydrazonoyl chloride **3** was prepared staring from N-*p*-Boc-phenylendiamine dissolved in MeOH that was first converted to its diazonium salt with $NaNO_2$/HCl and then by treatment with methyl-2-chloroacetoacetate in MeOH gave **3** in 55% yield (Scheme 1).

We next examined the conditions required for the cycloaddition of **1** with **2** and **3**. The cycloadditions were carried out in dry dioxane at 80 °C for 24 h using 2.5 equivalents of Ag_2CO_3 until complete conversion of **1**, which was always used in stoichiometric amount with respect to the dipoles (Scheme 2). The regioisomeric ratio was always calculated by ^{1}H NMR analysis of the crude mixtures using diagnostic signals. The identification of the 5-pyrazoles and the 4-pyrazoles was based on the ^{1}H NMR signals taking advantage from the CH signal on the C5 for the 4-substituted pyrazole which resonates at about 8.0 ppm as reported with X-ray analysis by us [24c].

As reported in Scheme 2, the 1,3-DC of **1** with **2** gave 5-substituted pyrazole **4** as the only regioisomer in 48% yield. Then we carried out the reduction of the nitro group with Pd/C (10% W/W) and ammonium formate in 60% yield and quantitatively the Boc removal with HCl/EtOAc giving **5** (**Target A**) as the dichlorhydrate salt.

In the case of **3**, its cycloaddition with **1** gave **6** in 64% yield as a mixture 80:20 of regioisomers 5-substituted/4-substituted with the 5-substituted being the major (Scheme 3). Despite several attempts it was not possible to isolate the minor isomer, because after several run on preparative TLC plates degradation was observed. Synthetic elaboration was therefore performed to isolate the target compound. Saponification with NaOH gave the corresponding carboxylic acid in 40% yield that was reacted in THF with N,N′-carbonyldiimidazole (CDI) and 2,3-dimethylaniline at room temperature for 3 h. An overall 48% yield for these two last steps was obtained for the pyrazole **7** (**Target B**).

2.4. In vitro kinase inhibition assay

Based on the docking results, the two compounds showed a potential affinity with several kinases suggesting a multi-kinase activity.

Both compounds were preliminarily tested against a panel of 20 human protein kinases [ALK, CDK2/cyclinA, CDK2/cyclinE, Flt3, GSK3-α, GSK3-β, IGF-1R, IKKβ, JAK2, JAK3, MAPK1, MAPK2, mTOR, PKBα, PKBβ, Src, PI3K(p110α/β/δ)] to assess their kinase inhibition (KinaseProfiler service; Millipore UK Ltd, UK) in the presence of 3 μM compound and 10 μM ATP. Results were presented as

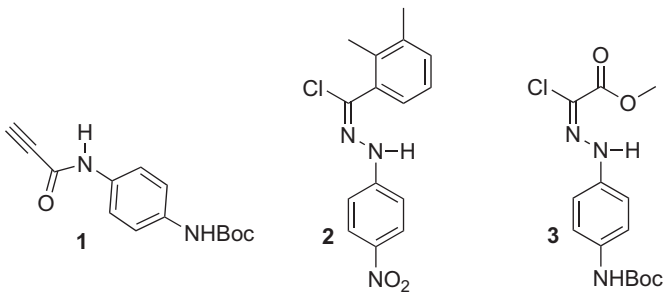

Scheme 1. Structures of dipolarophile **1** and precursors of the 1,3-dipoles **2** and **3**.

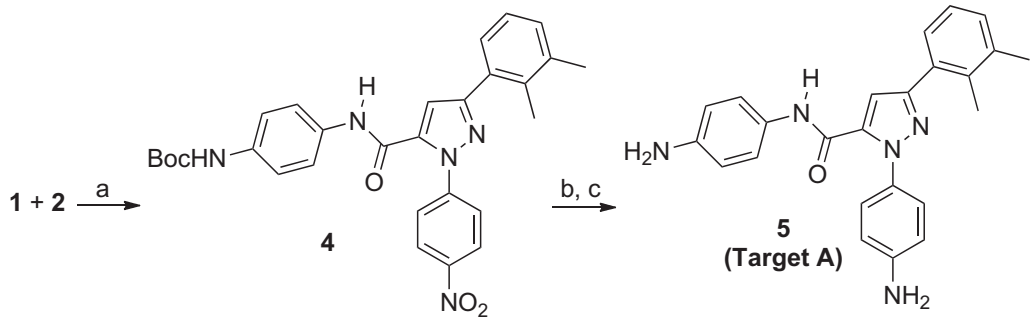

Scheme 2. 1,3-Dipolar cycloaddition of **1** with **2** and synthetic elaboration of the cycloadduct **4** for the synthesis of **5** (**Target A**). Reagents and conditions: (a) Ag_2CO_3, 1,4-dioxane, 80 °C, 24 h, 35%. (b) Pd-C, NH_4HCO_2, MeOH, 0 °C-1 h to rt overnight, 60%. (c) HCl 3 M in EtOAc, rt, 8 h, 100%.

percentage of inhibition compared to control; details of assay conditions used can be found at the website www.millipore.com.

At 3 μM concentration all the evaluated kinases were not inhibited by both compounds. So, the suggested concentrations for further *in vitro* biological activity started from 50 μM.

2.5. Antiproliferative effect and cytotoxicity

To define the biological activity, in terms of cell proliferation inhibition and cytotoxicity, the compounds, **5** and **7**, were tested in SNU449 cells at 50, 100 and 150 μM.

Evaluating the number of viable cells at 48 h after treatment, a decrease of total cell number was observed with both molecules at the concentration of 50 μM; in particular the effect on cell proliferation results more evident for **5** than **7**, comparing the number of viable cells to the control (Ctrl) cells. At 72 h of treatment, both compounds strongly reduced growth and exerted an evident cytotoxic effect. Analysing the percentage of viable cells after **5** and **7** treatment at the same concentrations, we could establish the IC_{50} for both compounds (Fig. 3). Compound **7**, as previously observed, showed a slower effect on the proliferation and the IC_{50} value is 150 μM at 48 h and around 50 μM at 72 h. Otherwise, the effect of **5** is stronger also at 48 h, where the IC_{50} value is less the 100 μM and at 72 h is less than 50 μM. Both the inhibitors after 72 h of treatment have an IC_{50} less than 50 μM.

2.6. Effect of 7 and 5 on PI3K/AKT pathway

Among the ATP-dependent kinases tested, our in silico (computational docking) analysis identified phosphoinositide-3-kinase (PI3K) and serine/threonine-protein kinase B (AKT) as hypothetical molecular targets of **7** and **5** kinase inhibitors. Since PI3K/AKT pathway is often deregulated in hepatocellular carcinoma and its involvement in HCC development and progression is well known [8], we investigated the biological effect of the two inhibitors on this molecular pathway. Firstly, we analyzed by Western blot the protein expression level of the serine–threonine protein kinase AKT in five HCC-derived cell lines. Indeed, AKT is one of the major downstream target of the kinase PI3K and its phosphorylation plays a key role in promoting cell proliferation and cell survival by the inactivation of Cyclin-Dependent Kinase (CDK) inhibitors and pro-apoptotic genes such as BAD [26]. We analysed both the total and the phosphorylated isoforms of AKT and we observed very different levels of its phosphorylation in the tested HCC cell lines (Fig. 4).

In particular, two cell lines, SNU449 and SNU475, displayed a very high extent of the phosphorylated AKT isoform (P-AKT). High phosphorylation levels in SNU449 and SNU475 cells let us to hypothesize a constitutive activation of the PI3K pathway in these cell lines. In the light of these data, we chose SNU449 cells to investigate the inhibitory effect of the two molecules on PI3K/AKT pathway, because the very high P-AKT expression levels in SNU475 cells could mask the inhibitory activity of our molecules or underestimate their true effect.

Initially, we studied the regulation of AKT phosphorylation following treatment with **7** and **5** compounds at three different concentrations (25–50–100 μM) in SNU449 cells. A decrease of P-AKT levels was observed with the two highest concentrations of tested molecules at both 48 and 72 h of treatment (Fig. 5A–B).

Since no alteration was observed at the lowest concentration, we chose the intermediate one to analyse if molecular changes could occur downstream of AKT pathway following the administration of **7** and **5** inhibitors. The 100 μM concentration was excluded to perform the subsequent analysis as it induced, especially with **5** molecule at 72 h, evident cell death and we supposed

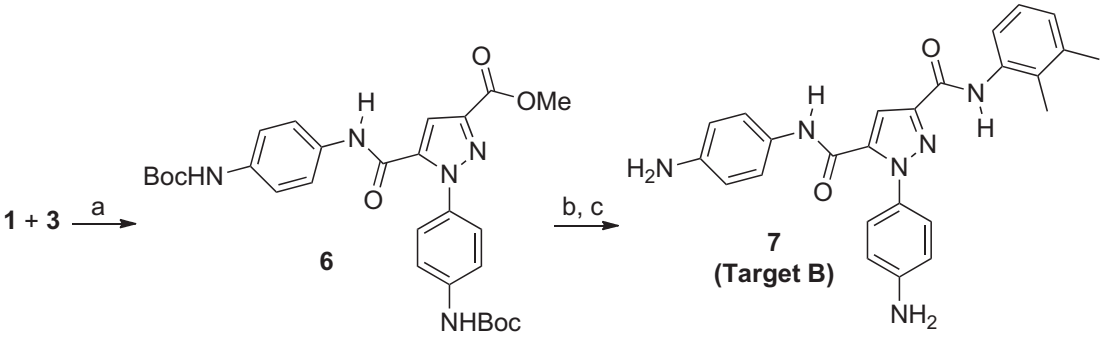

Scheme 3. 1,3-Dipolar cycloaddition of **1** with **3** and synthetic elaboration of the cycloadduct **6** for the synthesis of **7** (**Target B**). Reagents and conditions: (a) Ag_2CO_3, 1,4-dioxane, 80 °C, 24 h, 64%. (b) NaOH, MeOH, rt, overnight, 40%. (c) *N*,*N*-carbonyldiimidazole, THF, 2,3-dimethylaniline, rt, 2 h, 48%. HCl 3 M in EtOAc, rt, 8 h, 100%.

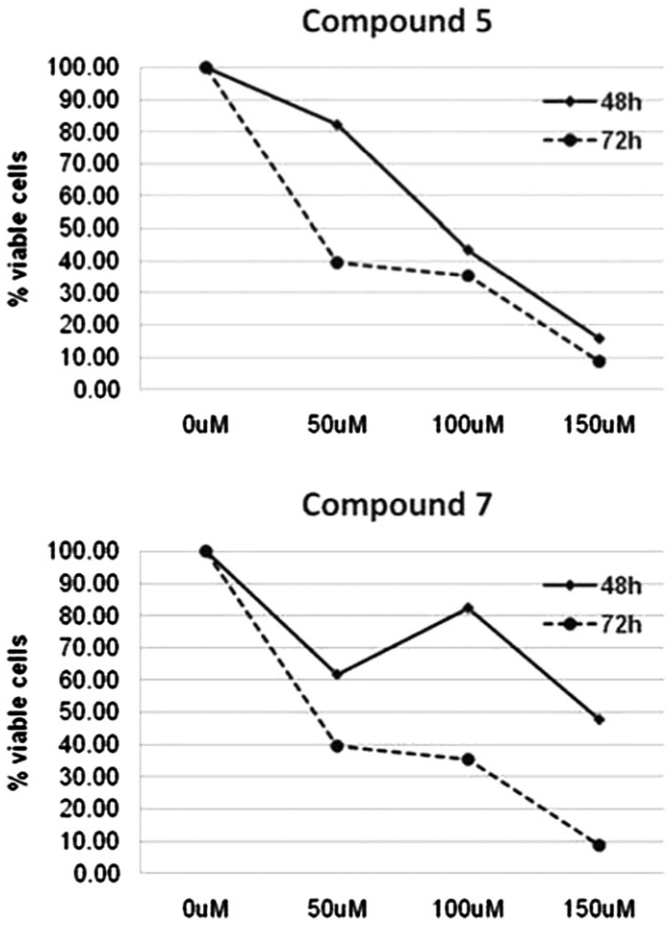

Fig. 3. Inhibitory activity of **5** and **7** on SNU449 HCC cell line after 48 h and 72 h of incubation with different compound concentrations.

that early regulation of molecular pathways could be hidden in this specific setting.

To investigate the functional activity of AKT kinase after treatment with the two inhibitors, the phosphorylation levels of both the direct and indirect AKT downstream effectors, glycogen synthase kinase 3 beta (GSK-3β) and ribosomal protein S6 (RpS6), was analysed in SNU449 cells. A decrease of the inhibitory phosphorylation (Ser-9) of GSK-3β was observed at 48 and 72 h with both molecules. In line with this finding a decrease of β-catenin protein levels were displayed in the same experimental settings. As regarding the PI3K/AKT/mTOR pathway, a decrease of the phosphorylated isoform of RpS6 was shown with both molecules and especially following administration of inhibitor **5** at 72 h. On the contrary, any inhibition of ERK1/2 phosphorylated isoform was revealed following treatment with **7** and **5** molecules (Fig. 6).

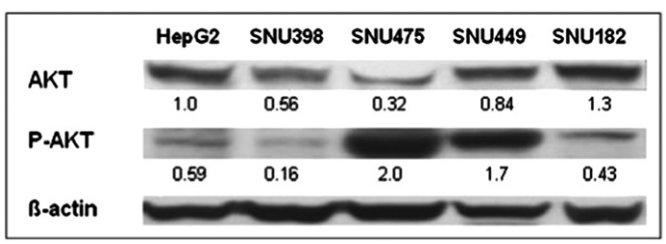

Fig. 4. Analysis of AKT in HCC-derived cell lines. Western blot analysis of AKT and P-AKT expression levels in HCC-derived cell lines. ß-actin was used as housekeeping gene. Numbers represent the ratio between AKT or P-AKT and β-actin expression.

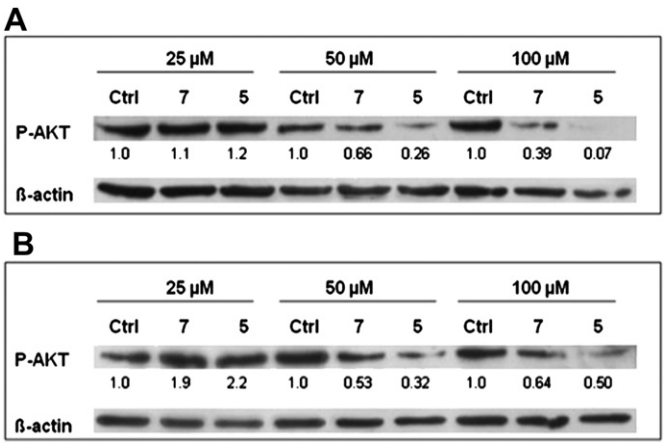

Fig. 5. P-AKT expression following treatments with **7** and **5**. Western blot analysis of P-AKT levels in SNU449 cells treated with **7** and **5** for 48 h (A) and 72 h (B). ß-actin was used as housekeeping gene. Numbers represent the ratio between P-AKT and β-actin expression. Ctrl represent cells treated with DMSO.

These findings demonstrated that the two tested molecules deregulate the PI3K/AKT pathway with a consistent decrease of the AKT kinase activity resulting in a down-regulation of the phosphorylation of its downstream target genes.

2.7. Cell cycle regulation by **7** and **5** molecules in SNU449 cells

To further characterize the biological role of the tested molecules, we analysed the cell cycle distribution following their administration in HCC cells. SNU449 cell line was treated with **7** and **5** at three different concentrations (25–50–100 μM) for 48 and 72 h. Cytofluorimetric analysis showed an inhibitory activity of cell cycle progression with an increase of the G1 phase cell population and a correspondent decrease of the S phase. In particular, treatment with the lowest concentration of **5** (25 μM) determined a G1 phase arrest at both 48 and 72 h. Regarding **7**, it exerted a cell cycle regulation at a higher concentration and a longer incubation time than **5**, especially it arrested cells in the G1 phase at a concentration of 50 μM following 72 h of treatment. At the highest concentration tested (100 μM), both the two molecules played a role in cell cycle regulation of SNU449 cells, with a marked increase of the G1 phase and a decrease of the S phase both at 48 and 72 h (Fig. 7A).

Subsequently, we evaluated by Western blot which cell cycle modulators could be involved in the arrest of SNU449 cells at the G1 checkpoint following treatment with the two molecules. To this aim, we tested the treatment with the intermediate concentration (50 μM) at 72 h, when both molecules exerted an inhibitory effect on cell cycle progression.

In agreement with FACS analysis, a decrease of cyclin D1 (CCND1) protein level was obtained after treatment with **7** and **5** compounds. In addition, an up-regulation of the cell cycle inhibitor CDKN1A/p21 was observed for both tested molecules, whereas no changes were shown for CDKN1B/p27. To deeply investigate which molecular pathways could be involved in cell cycle modulation, we analysed the protein expression level of the principal CDKN1A/p21 transcriptional regulator, p53. In accordance with CDKN1A/p21 up-regulation, an increase of p53 expression levels was observed following treatment with **7** and **5** compounds in SNU449 cells (Fig. 7B).

In order to try to explain the increase of p53 protein levels following treatment with **7** and **5**, we analysed the phosphorylation levels of the principal p53 inhibitor, MDM2. In particular, we

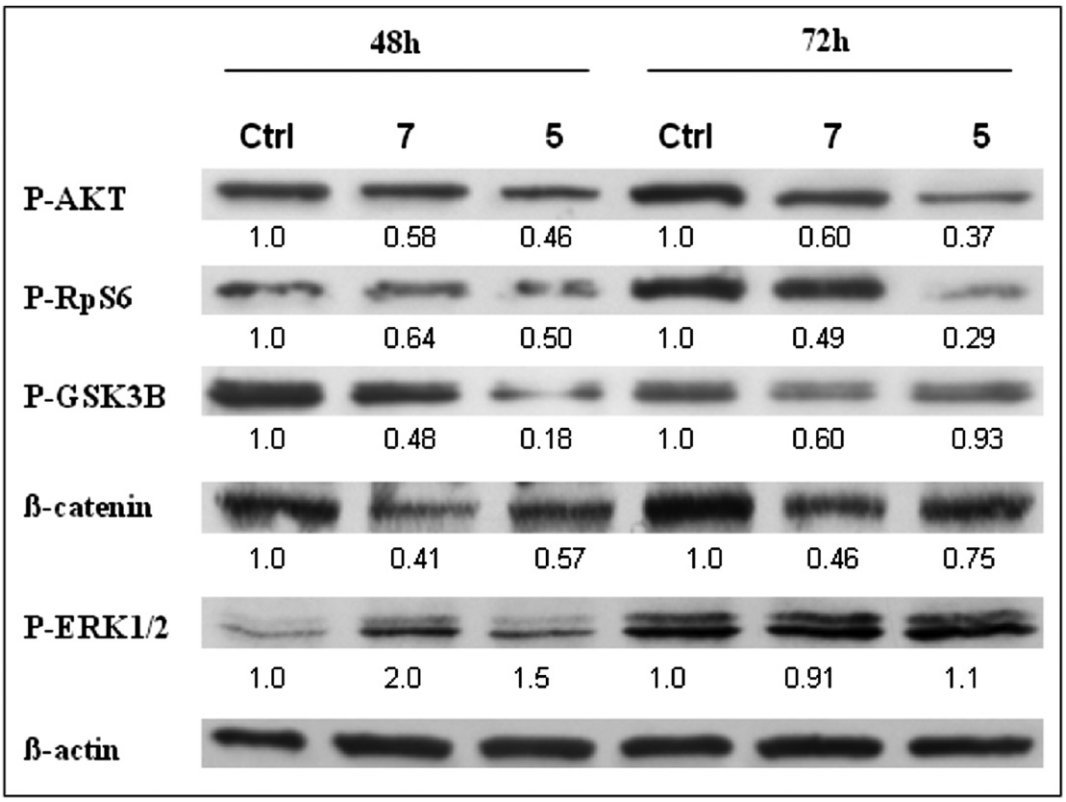

Fig. 6. Analysis of AKT targets following treatments with **7** and **5**. Western blot analysis of P-AKT, P-RpS6, P-GSK-3β, β-catenin and P-ERK172 levels in SNU449 cells treated with 50 μM of **7** and **5** compounds for 48 and 72 h -actin was used as housekeeping gene. Numbers represent the ratio between phosphorylated proteins and β-actin expression. Ctrl represent cells treated with DMSO.

investigated the phosphorylation levels of Ser-166 which is directly phosphorylated by the AKT kinase. This phosphorylation determines MDM2 activation, allowing its entry into the nucleus where it targets p53 for degradation. Western blot analysis showed a decrease of phosphorylated-MDM2 isoform in SNU449 cells treated with both inhibitory compounds, whereas the levels of total MDM2 remained unchanged (Fig. 7B).

Taken together, these findings demonstrated that the two inhibitors play an active role in cell cycle modulation of HCC cells, at least in part through the down-regulation of MDM2 phosphorylation and an activation of p53 transcriptional activity and the inhibition of WNT/β-catenin pathway.

*2.8. Apoptotic cell death is triggered by treatment with **7** and **5** compounds in SNU449 cells*

After 72 h of treatment with the two molecules at 50–100 μM, SNU449 cells displayed a decreased growth rate and an increased cell death (Fig. 8A).

To characterize if programmed cell death, apoptosis, was responsible for decreased SNU449 cell number following **7** and **5** administration, a FACS-Annexin V assay was performed. This assay showed an increase of apoptosis following treatment with **5** inhibitor at both 50 and 100 μM concentrations. Regarding **7** molecule, a trend toward increased apoptotic cell death was displayed, even if it did not reach the statistical significance. Following treatment with the two compounds, the low and almost unchanged Propidium Iodide (PI) incorporation confirmed that apoptotic cell death is an early event in SNU449 cells at the tested concentrations (Fig. 8B).

3. Conclusions

The preliminary docking investigation for a rationale development of our 3,5-pyrazole derivatives with potential affinity and selectivity toward different kinases, suggested that a potential effective inhibitory molecule to the ATP kinase binding site could be attained by the following structural features: (1) C-3 hydrophobic aryl moiety; (2) pyrazole moiety with amino-phenyl substituent at N1 and lateral aminophenyl substituents in the 5–CO–NH-R. The common binding mode of the two derivatives into the ATP binding site through two possible relevant hydrogen-bonding interactions and a complementary apolar interaction surface could explain the inhibitory activity of our two compounds in HCC cell lines. The introduction of a carboxamide group in position 3 of **7,** connected with the dimethyl-phenyl group, did not improve the inhibitory activity.

The binding pose of **5** and **7** – obtained with docking results – within ATP binding site of the evaluated kinases, suggest that the two compounds are aspecific ATP competitors. *In vitro* study confirmed inhibitory effect - at micromolar concentrations - against the HCC-derived cell line SNU449, after an incubation of 48 and 72 h. The more favourable logP partition coefficent of **5** (logP equal to 4.47) in comparison with that of **7** (logP equal to 3.27) could explain the better *in vitro* results due to more lipophilic characteristic, suggesting a more easily entrance of the compound inside the cells.

Here we demonstrated that **7** and **5** exert an inhibitory activity on the PI3K/AKT/mTOR pathway resulting in a down-regulation of the phosphorylated isoform of both direct and indirect downstream targets such GSK-3β, ribosomal subunit S6 and MDM2. The unselective action of the two compounds against multiple kinases was ruled out by testing ERK1/2 phosphorylation, whose levels did not change after treatment with both **7** and **5**.

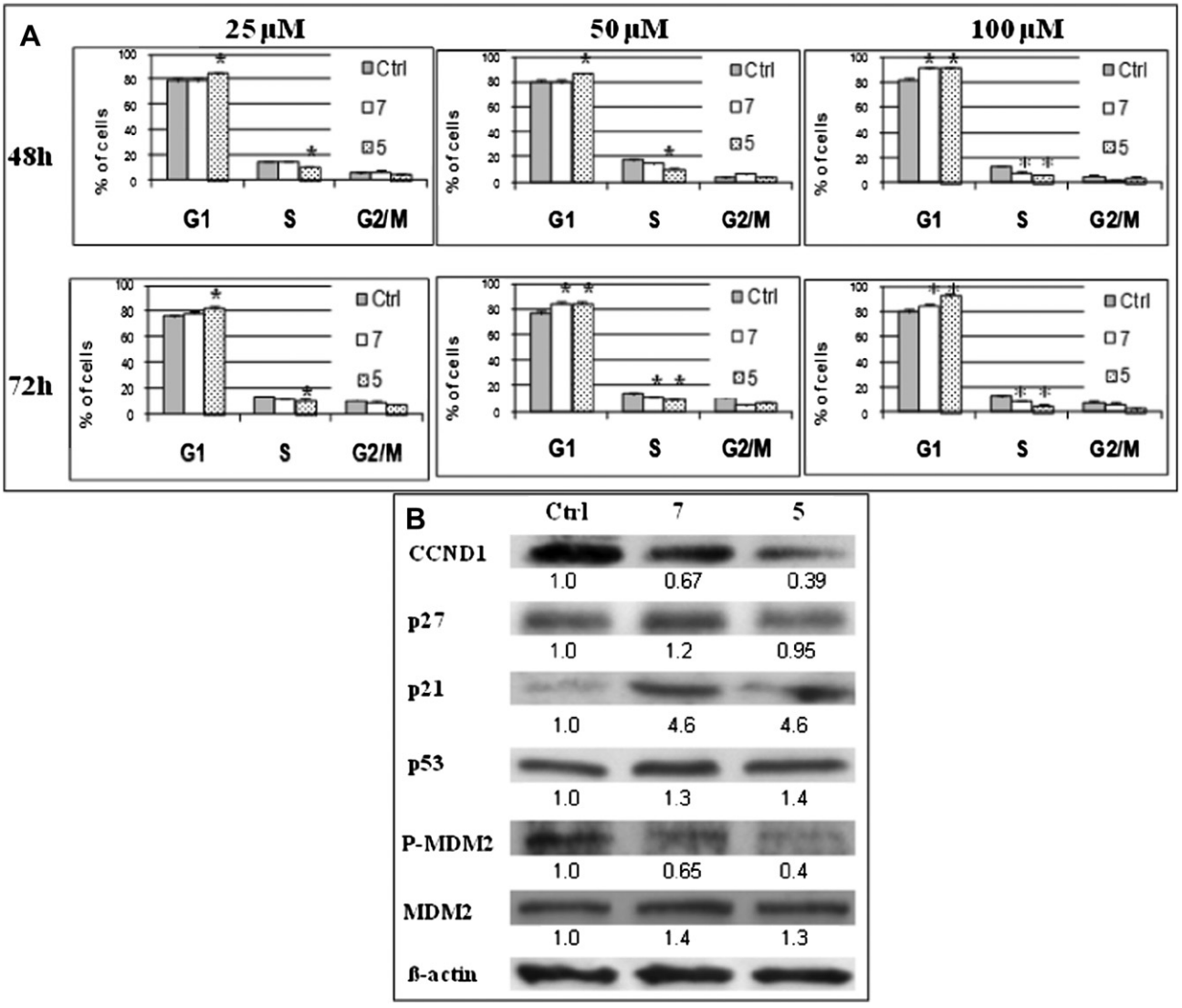

Fig. 7. Compounds **5** and **7** affect cell cycle. (A) Analysis of cell cycle variations induced by different concentrations of **5** and **7** in SNU449 cells for 48 and 72 h. Controls (Ctrl) represent cells treated with DMSO. Columns, average values; bars, SD. *means $p < 0.05$. (B) Western blot analysis of cell cycle regulators, p53, MDM2 and P-MDM2 in SNU449 cells treated with 50 μM of **7** and **5** for 72 h -actin was used as housekeeping gene. Numbers represent the protein expression ratio between the analyzed genes and β-actin.

Moreover, the tested compounds determined a block of cell cycle in the G1 phase, with a correspondent decrease of the S and G2/M phases. In accordance with a decrease of AKT kinase activity, observed in SNU449 cells treated with **7** and **5** molecules, a down-regulation of phosphorylation levels of MDM2 protein at Ser-166 was also reported. We suggest that a decrease of phosphorylated-MDM2 isoform is responsible for p53 increased expression which, in turn, transcriptionally activates its target gene, CDKN1A/p21 [27] and that the block of cell cycle observed in SNU449 cells treated with the two molecules might be ascribed, at least in part, to the activation of CDKN1A/p21. To further characterise the effects of **7** and **5**, cyclin D1 protein levels were investigated and their decrease in treated cells proved a direct effect of the two compounds on cell proliferation. This might be related with the activation of GSK-3β, which in turn phosphorylates β-catenin leading to its ubiquitination and degradation.

Microscopical view of SNU449 cells following 72 h of treatment with **7** and **5** showed both a decrease of cell proliferation and cell death, suggesting a contemporaneous cytostatic and cytotoxic effect. The nature of cell death was investigated by a cytofluorimetric analysis which demonstrated that both compounds, in particular **5**, triggered apoptosis in HCC-derived cells.

Therefore, this synthetic protocol will offer a general entry to 3,5-disubstituted pyrazoles having in position 3 both aromatic and amidic functional group, as a new strategy to inhibit the PI3K/AKT/mTOR pathway in HCC which might improve the drug response to molecularly-targeted therapy agents. These compounds could therefore be considered as leads for SAR development.

4. Experimental

4.1. Material and methods

^{1}H NMR and ^{13}C NMR spectra were recorded using $CDCl_3$ or CD_3OD or DMSO-d_6 solutions at 300, 400 and 600 MHz for ^{1}H and 75.46, 100.6 and 150.92 MHz for ^{13}C. Chemical shifts (δ) are reported in ppm relative to $CHCl_3$ ($\delta = 7.26$ for ^{1}H and $\delta = 77.0$ for ^{13}C). *J* values are given in Hz. ^{1}H NMR and ^{13}C NMR spectral assignments were made by DEPT, gCOSY and gHSQC experiments. IR spectra were recorded in solvent as specified. Mass spectra (MS) were

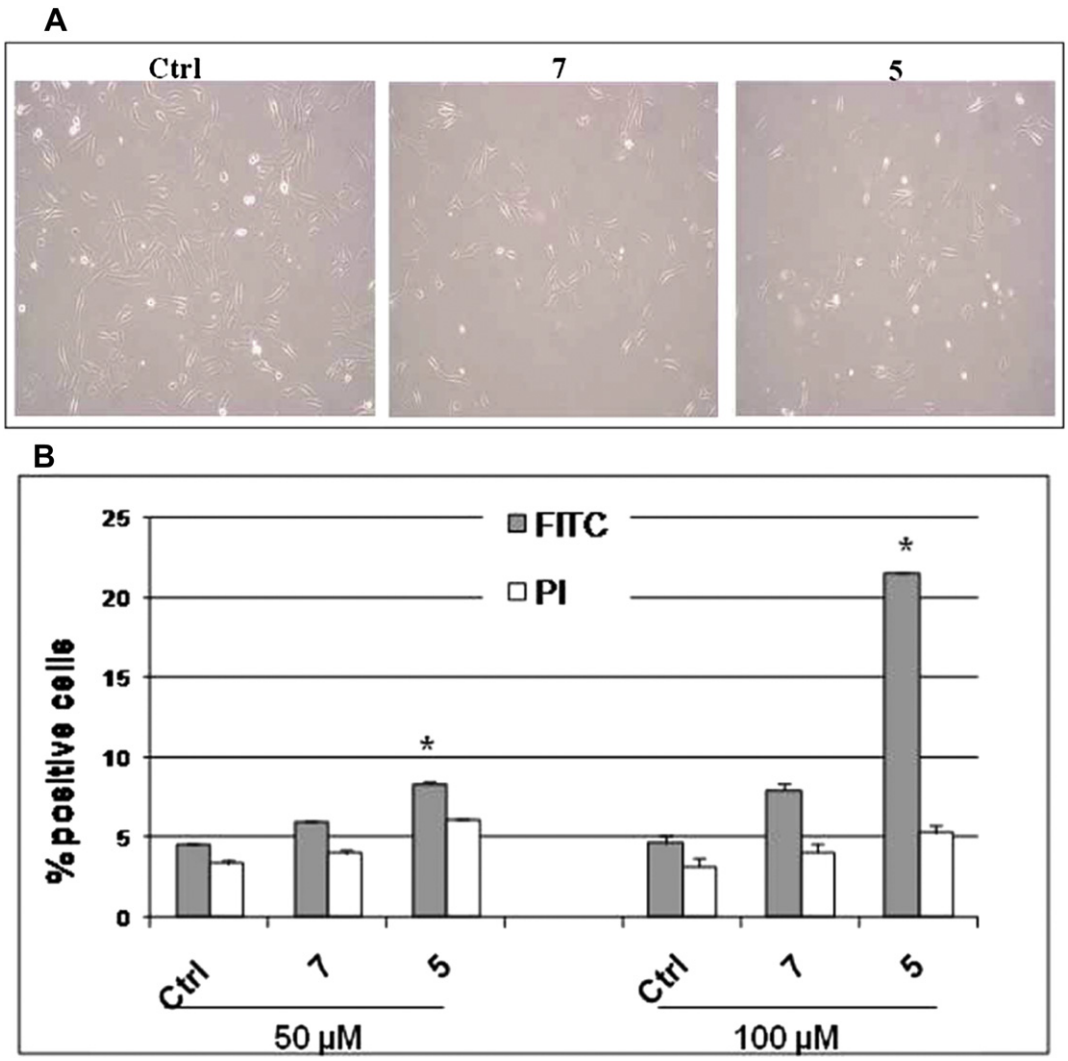

Fig. 8. Compounds **5** and **7** trigger apoptosis. (A) Microscopic view of SNU449 cells treated with 100 μM of **5** and **7** or vehicle molecule (Ctrl). Original magnification, X10. (B) FACS-Annexin V analysis of SNU449 cells treated with different concentrations of **7** and **5** for 72 h. Columns, average values; bars, SD. *means $p < 0.05$.

obtained with an electrospray ionization source (ESI-MS). All the ESIMS spectra were performed using MeOH as the solvent. High Resolution Mass Spectra (HRMS) were recorded on a micromass LCT spectrometer using electrospray (ES^+) ionisation techniques. Reactions were conducted in oven-dried (120 °C) glassware under a positive Ar atmosphere. Transfer of anhydrous solvents or mixtures was accomplished with oven-dried syringes/septum techniques. THF was distilled from sodium/benzophenone just prior to use and stored under Ar. Toluene was distilled from sodium. Et_2O was distilled from phosphorus pentoxide. CH_2Cl_2 was passed through basic alumina and distilled from CaH_2 prior to use. Other solvents were purified by standard procedures. Light petroleum ether refers to the fraction with bp 40–60 °C. The reactions were monitored by TLC performed on silica gel plates (Baker-flex IB2-F). Column chromatography was performed with Merck silica gel 60 (70–230 mesh). Preperative TLC was carried out on glass plates using a 1 mm layer of Merck silica gel 60 Pf 254. All chemicals were used as obtained or purified as needed.

4.2. Chemistry

Tert-butyl-(4-propiolamidophenyl)carbamate **1**: In a two-neck round-bottom flask, under stirring and nitrogen, 1.60 mL (26 mmol) of propiolic acid and 13 mL of diethyl ether were added. The temperature was lowered to °C, 5.4 g (26 mmol) of DCC were slowly added followed by 37 mg (0.3 mmol) of DMAP. N-*p*-Boc-phenylendiamine (5.4 g, 26 mmol) in 25 mL of THF was slowly added. The reaction was stirred for 24 h at 35 °C. The mixture was filtered over celite and the THF was removed *in vacuo*, EtOAc (10 mL) was added, the organic phase was dried over Na_2SO_4 and the crude was purified by column chromatography on silica gel (petroleum ether:EtOAc 2:1) giving 4.87 g (72%) of **1** as a yellow solid. M.p.: 174–176 °C. MS (EI, *m*/*z*) 260 (M+). ^{1}H NMR ($CDCl_3$, 400 MHz) δ: 1.52 (s, 9H, CH_3), 2.92 (s, 1H, CH), 6.48 (brs, 1H, NH), 7.52 (brs, 1H, NH), 7.32 (d, $J = 8,8$ Hz, 2H, CH), 7.44 (d, $J = 8,8$ Hz, 2H, CH).

(*E*)-2,3-Dimethyl-*N*′-(4-nitrophenyl)benzohydrazonoyl chloride **2**: In a two-neck round-bottom flask, under stirring and nitrogen, 3.0 g (20 mmol) of 2,3-dimethylbenzoic acid were added and the mixture was refluxed with 3.62 mL (50 mmol) of $SOCl_2$. After 8 h the excess of $SOCl_2$ was removed at the rotavapor and under *vacuum* to give the 3,3-dimethyl benzoyl chloride as a yellow oil in quantitative yield that was used further without purification.

In a two-neck round-bottom flask, under stirring and nitrogen, were added 307 mg (2 mmol) of *p*-nitrophenyl hydrazine, 227 μL (2 mmol) of triethylamine and 5 mL of THF. The temperature was lowered to 0 °C, 2,3-dimethylbenzoylchloride (2.0 mmol) was

slowly added in 15 mL of THF and the reaction mixture was stirred at room temperature for 4 h. THF was removed under reduced pressure, EtOAc was added (10 mL) and the organic layer was washed with water 5 times (5 mL each). The organic phase was dried over Na_2SO_4 and the crude was crystallized with EtOH giving 428 mg (75%) of 2,3-dimethyl-*N*′-(4-nitrophenyl)benzohydrazide as an orange solid. M. p. = 275–277 °C. MS (ESI) 308 (M^+ + Na), 284 (M^+-1). ^{1}H NMR (CD_3OD, 400 MHz) δ: 2.55 (s, 3H), 2.57 (s, 3H), 6.92 (d, J = 9.0 Hz, 2H), 7.09 (m, 3H), 8.14 (d, J = 9.0 Hz, 2H).

The above reported 2,3-dimethyl-N′-(4-nitrophenyl) benzohydrazide (571 mg, 2 mmol) was dissolved in acetonitrile (3.0 mL), then 656 mg (2.50 mmol) of triphenylphosphine and 242 μl (2.50 mmol) of CCl_4 were added. After stirring for 24 h at room temperature the crude was purified on column chromatography on silica gel (petroleum ether: EtOAc 3:1) giving 425 mg (70%) of **2** as a yellow solid. M. p. = 210–211 °C. MS (ESI): 284 (M^+-1). ^{1}H NMR ($CDCl_3$, 300 MHz) δ: 2.36 (s, 3H, CH_3), 2.40 (s, 3H, CH_3), 7.15 (d, J = Hz, 2H, CH), 7.19 (d, J = 9 Hz, 1H, CH), 7.25 (d, J = 7 Hz, 1H, CH), 7.38 (d, J = 9 Hz, 1H, CH), 8.20 (d, J = 9 Hz, 2H, CH), 8.38 (s, 1H, NH). ^{13}C NMR ($CDCl_3$, 100 MHz) δ: 16.9, 20.5, 112.5, 125.5, 126.0, 127.36, 128.3, 131.5, 134.8, 135.3, 137.9, 141.2, 148.3.

(*Z*)-methyl-2-(2-(4-((tert-butoxycarbonyl)amino)phenyl) hydrazono)-2-chloacetate **3**: Prepared according to reference 24a. Starting from N-*p*-Boc-phenylendiamine (3.12 g, 15 mmol) to give 2.7 g (55%) of **3** as a yellow sticky oil that was used further without purification. ESI-MS: 350 [M^+ + Na]. ^{1}H NMR ($CDCl_3$, 400 MHz) δ: 8.31 (s, 1H), 7.35 (d, J = 22 Hz, 2H), 7.17 (d, J = 22 Hz, 2H), 6.42 (s, 1H), 3.92 (s, 3H), 1.51 (s, 9H).

*4.2.1. General procedure for the 1,3-DC of **1** with **2** and **3***

To a solution of **1** (1 mmol) and the precursor of the 1,3-dipoles **2** or **3** (1 mmol) in 1,4-dioxane (4.4 mL) was added Ag_2CO_3 (0.69 g, 2.5 mmol) and the reaction mixture was stirred at 80 °C for 24 h. The reaction was filtered over celite and the solvent was removed under vacuum. Purification and characterization was carried out as reported below.

4.2.2. General procedure for the Boc deprotection

The Boc deprotection was performed starting from 0.5 mmol of product dissolved in EtOAc (5 mL) and adding 0.5 mL of 3 M HCl in EtOAc. After 2–8 h at room temperature (following by TLC), the solvent was evaporated to yield pure products as chlorohydrate, then the free amine was obtained after basification with *conc*. Ammonia and extraction with EtOAc.

*4.2.2.1. Synthesis of N,1-bis(4-aminophenyl)-3-(2,3-dimethylphenyl)-1H-pyrazole-5-carboxamide **5**.* Tert-butyl (4-(3-(2,3-dimethylphenyl)-1-(4-nitrophenyl)-1*H*-pyrazole-5-carboxamido)phenyl)carbamate **4**: Starting from **2** (421 mg, 1.4 mmol), **1** (361 mg, 1.4 mmol). Purification on column chromatography on silica gel (petroleum ether:EtOAc 3:1) gave **4** as a yellow sticky oil. Yield: 35%. MS (ESI) 550 (M^+ + Na). ^{1}H NMR ($CDCl_3$, 300 MHz) δ: 1.52 (s, 9H, CH_3), 2.36 (s, 3H, CH_3), 2.40 (s, 3H, CH_3), 6.51 (br s, 1H, NH), 6.96 (s, 1H, CH), 7.20 (m, 3H, CH), 7.36 (d, J = 8.1 Hz, 2H, CH), 7.50 (d, J = 8.7 Hz, 2H, CH), 7.78 (d, J = 9 Hz, 2H, CH), 7.87 (brs, 1H, NH), 8.31 (d, J = 9 Hz, 2H, CH). ^{13}C NMR ($CDCl_3$, 75 MHz) δ: 17.3, 20.9, 28.5, 80.9, 110.6, 119.2, 121.1, 124.4, 125.1, 125.7, 127.6, 130.5, 131.6, 131.9, 135.0, 135.7, 137.4, 137.8, 144.6, 146.7, 152.7, 154.0, 157.2.

In a two-neck round-bottom flask, under stirring and nitrogen, **4** (458 mg, 0.9 mmol) was dissolved in MeOH (9 mL). The temperature was lowered to °C, then 86.8 mg of Pd/C (10% w/w) and ammonium formate (547 mg, 9 mmol) were added. The mixture was stirred 1 h at °C and then overnight at room temperature. The crude was filtered over celite and purified on column chromatography on silica gel (petroleum ether: EtOAc 2:1) giving 269 mg (60%) of tert-butyl (4-(1-(4-aminophenyl)-3-(2,3-dimethylphenyl)-1*H*-pyrazole-5-carboxamido)phenyl)carbamate as a white sticky solid. MS (ESI) 498 (M + 1), 520 (M^+ + Na), 536 (M + K). ^{1}H NMR (CD_3OD, 300 MHz) δ: 1.51 (s, 9H, CH_3), 2.34 (s, 3H, CH_3), 2.38 (s, 3H, CH_3), 6.76 (d, J = 8.7 Hz, 2H, CH), 6.95 (s, 1H, CH), 7.16 (m, 2H, CH), 7.25 (d, J = 8.7 Hz, 2H, CH), 7.34 (m, 3H, CH), 7.46 (d, J = 9 Hz, 2H, CH), 7.90 (s, 1H, NH), 8.92 (brs, 1H, NH). ^{13}C NMR (CD_3OD, 75 MHz) δ: 17.2, 20.8, 28.7, 80.8, 109.8, 115.8, 119.9, 122.2, 126.3, 126.9, 128.6, 130.8, 131.4, 133.7, 133.8, 135.92, 137.3, 138.4, 139.1, 149.3, 153.3, 155.1, 160.2.

N,1-bis(4-aminophenyl)-3-(2,3-dimethylphenyl)-1*H*-pyrazole-5-carboxamide ***5***: Starting from 324 mg (0.65 mmol) of tert-butyl (4-(1-(4-aminophenyl)-3-(2,3-dimethylphenyl)-1*H*-pyrazole-5-carboxamido)phenyl)carbamate. Compound **5** was obtained in 100% yield as a white solid. Characterization was carried out after basification with conc. ammonia and extraction with EtOAc. M.p.: 243–246 °C. MS (ESI). 398 (M+1), 420 (M^++Na). ^{1}H NMR (CD_3OD, 400 MHz) δ: 2.35 (s, 3H, CH_3), 2.41 (s, 3H, CH_3), 7.19 (m, 2H, CH), 7.26 (s, 1H, CH), 7.37 (d, J = 7.6 Hz, 1H, CH), 7.41 (d, J = 8.8 Hz, 2H, CH), 7.57 (d, J = 8.4 Hz, 2H, CH), 7.64 (s, 1H, NH), 7.73 (d, J = 8.8 Hz), 7.85 (d, J = 8.8 Hz, 2H, CH). ^{13}C NMR (CD_3OD, 100 MHz) δ: 17.2, 20.7, 111.8, 123.0, 124.7, 124.9, 126.6, 127.8, 128.7, 131.5, 131.5, 133.3, 136.1, 138.6, 140.2, 141.9, 154.7, 159.9. Anal. Calcd for C24H23N5O: C, 75.52; H, 5.83; N, 17.62. Found: C, 75.48; H, 5.85; N, 17.63.

*4.2.2.2. Synthesis of N^5,1-bis(4-aminophenyl)-N^3-(2,3-dimethylphenyl)-1H-pyrazole-3,5-dicarboxamide **7**.* Methyl 1-(4-((tert-butoxycarbonyl) amino)phenyl)-5-((4-((tert-butoxycarbonyl) amino)phenyl)carbamoyl)-1*H*-pyrazole-3-carboxylate **6**: Starting from **3** (645 mg, 2.0 mmol), **1** (520 mg, 2.0 mmol). The cycloaddition gave a ratio 4/1 in favour of the major isomer. Purified on column chromatography on silica gel (petroleum ether: EtOAc 1:1) as a yellow oil. Yield: 64%. ESI-MS: 574 [M^+ + Na]. ^{1}H NMR ($CDCl_3$, 300 MHz) δ: 1.50 (s, 9H), 1.51 (s, 9H), 3.95 (s, 3H), 6.50 (s, 1H), 6.68 (s, 1H), 7.36–7.40 (m, 2H), 7.45–7.50 (m, 2H), 7.52 (s, 1H), 7.67 (d, J = 30 Hz, 2H), 7.71 (d, J = 30 Hz, 2H), 8.63 (s, 1H). ^{1}H NMR ($CDCl_3$, 300 MHz) δ: 28.5 (br), 80.0 (br), 120.1–123.2 (Ar CH), 133., 133.6, 135.1, 135.4 (Ar C(IV)), 152.5, 152.7, 160.3, 162.6. Minor isomer methyl 1-(4-((tert-butoxycarbonyl) amino)phenyl)-4-((4-((tert-butoxycarbonyl)amino)phenyl)carbamoyl)-1*H*-pyrazole-3-carboxylate. Attempted purification failed to produce pure compound, only a ^{1}H NMR could be extrapolated but some impurities, derived from degradation on plates, were always present. ^{1}H NMR ($CDCl_3$, 300 MHz) δ: 1.50 (s, 9H), 1.51 (s, 9H), 4.07 (s, 3H), 6.59 (s, 1H), 6.85 (s, 1H), 7.36–7.45 (m, 2H), 7.60–7.65 (m, 2H), 7.70–7.75 (m, 2H), 8.65 (s, 1H).

In a two-neck round-bottom flask, under stirring and nitrogen, compound **6** (1.33 g, 2.41 mmol) was dissolved in 16 mL of MeOH and 4 mL of a 2 M solution of NaOH were added. The reaction was stirred overnight at room temperature and then methanol was eliminated. Et_2O was added (5 mL) and the organic layer was washed twice with water (5 mL). The pH was adjusted to 4 with HCl *conc*. The acidic layer was extracted twice with EtOAc (5 mL) and once with chloroform (5 mL). The combined organic phases were dried over Na_2SO_4, filtered, concentrated and dried under vacuum giving 1-(4-((tert-butoxycarbonyl)amino)phenyl)-5-((4-((tert-butoxycarbonyl) amino) phenyl)carbamoyl)-1*H*-pyrazole-3-carboxylic acid as a brown solid (40%) that was used without further purification. ESI-MS: 560 [M^+ + Na].

In a two-neck round-bottom flask, under stirring and nitrogen, 1-(4-((tert-butoxycarbonyl)amino)phenyl)-5-((4-((tert-butoxycarbonyl)amino)phenyl)carbamoyl)-1*H*-pyrazole-3-carboxylic acid (490 mg, 0.91 mmol) was dissolved in THF (4 mL). Slowly, *N*-*N*-carbonyldiimidazole (200 mg, 1.25 mmol) was added and the reaction was stirred at room temperature for 1 h 2,3-dimethylaniline (223 μL, 1.25 mmol) in 1.5 mL of THF was added

and the mixture was stirred for 2 h. The solvent was removed under reduced pressure, EtOAc (10 mL) was added and the organic layer was washed with HCl 1 M (5 mL). The organic phase was dried over Na_2SO_4 filtered, concentrated and dried under *vacuum* giving a crude that was purified on column chromatography on silica gel (petroleum ether: EtOAc 2:1) as a yellow oil giving the corresponding amide (48%) as a sticky yellow solid. ESI-MS: 663 [$M^+ + Na$]. ^1H NMR ($CDCl_3$, 300 MHz) δ: 1.51 (s. 9H), 1.53 (s, 9H), 2.20 (s, 3H), 2.29 (s, 3H), 6.45 (s, 1H), 6.67 (s, 1H), 6.98–7.10 (m, 2H), 7.39–7.49 (m, 9H), 7.60–7.70 (m, 2H), 8.26 (s, 1H), 8.66 (s, 1H).

Following the general procedure for the Boc removal. Starting from the above reported amide (107 mg, 0.17 mmol). N^5,1-bis(4-aminophenyl)-N^3-(2,3-dimethylphenyl)-1*H*-pyrazole-3,5-dicarboxamide **7** was isolated as a white solid. Yield: 100%. M. p.: >300 °C dec. Characterization was carried out after basification with *conc.* ammonia and extraction with EtOAc. ESI-MS: 463 [$M^+ + Na$]. ^1H NMR (DMSO-d_6, 400 MHz) δ: 2.15 (s, 3H), 2.32 (s, 3H), 7, 14–7.18 (m, 1H), 7.26–7.30 (m, 1H), 7.35–7.38 (m, 2H), 7.41–7.45 (m, 2H), 7.62–7.65 (m, 2H), 7.72 (s, 1H), 7.84–7.90 (m, 2H), 9.97 (s, 1H), 10.85 (s, 1H). ^{13}C NMR (DMSO-d_6, 100 MHz) δ: 14.8, 20.8, 110.6, 121.8, 124.3, 124.8, 125.9, 127.3, 128.2, 132.8, 136.3, 136.8, 137.6, 138.7, 138.9, 147.0, 157.7, 160.0. Anal. Calcd for C25H24N6O2: C, 68.17; H, 5.49; N, 19.08. Found: C, 68.14; H, 5.46; N, 19.95.

4.3. Molecular docking

The following operating procedures were followed for the development of the 3,5-pyrazole derivatives: (a) geometry optimization of the proposed ligands; (b) virtual docking of the proposed pyrazole derivatives to calculate their predicted binding energy to the active site of several kinases.

4.3.1. Preparation of molecules

Before starting the docking calculations, ligand geometry optimization was done by semi-empirical AM1 [28] of the minimum-energy conformation using Gaussian 3 [29].

4.3.2. Preparation of target macromolecule

The target proteins AKT2 (PDB: 2jdr), GSK3β (PDB: 1pyx), PI3K (PDB: 2v4l), CDK2 (PDB: 2j9m), AurA (PDB: 2x6d), MAPKJ (PDB: 2pzy), EGFR (PDB: 2rpg), IGFR (PDB: 2zm3), were retrieved from the Protein Data Bank (http://www.rcsb.org/pdb/). The proteins were prepared with Maestro 9.1 software (Schrödinger, LLC, New York, NY, 2010) deleting waters, optimizing H-Bond assignments and deleting original ligands.

4.3.3. Procedure for molecular docking

Docking calculations were carried out using AutoDock 4.1 [25] and Autogrid 4.0 on a dual-xeon T7400 Dell workstation. Grids (one grid for each atom type in the ligand, plus an electrostatic and a desolvation map) were centred on the binding site and were chosen to be large enough (70 × 70 × 70 A°) to allow the ligand to rotate freely, even in its most fully-extended conformation.

Docking was performed using the AutoDock empirical free energy function and the Lamarckian genetic algorithm with local search. Lamarckian genetic algorithms can handle ligands with more degrees of freedom than the simulated annealing method.

One hundred fifty docking runs with 2.500.000 energy evaluations for each run were performed for each molecule and all the evaluated kinases. Cluster analysis (RMS tolerance equal to 0.5 Å) was then carried out on the docked results. Inhibitors were compared according to the cluster with lowest docked energy found. The inhibition constants – Ki – were calculated from the docked energy.

4.4. Biological assays

4.4.1. Cell culture and treatments

HepG2 cell line was cultured with Minimum Essential Medium (Eagle) while SNU398, SNU182, SNU449 and SNU475 cell lines were cultured with RPMI 1640; both media were supplemented with 10% foetal bovine serum (FBS) and antibiotics. Cells were treated at different concentrations (range 25–150 μM) of the two compounds for 24, 48 and 72 h and cells were collected for Western blot and FACS analysis.

4.4.2. Cytotoxicity assay

Exclusion test of cell viability was performed using trypan blue (TB) viable cell counts protocol (Shapiro, H.M. 1988 [30]). Pyrazoles were dissolved in dimethylsulphoxide (Sigma–Aldrich, Saint Louis, MO) at 10 mM stock concentration, then diluted. SNU449 cells were treated with pyrazoles or DMSO (as control) at different concentrations for 48 and 72 h and in triplicate. Then 0.4% TB solution was added to each well following the standard protocol procedure. Cell countings were performed using a Burker chamber. Triplicate values were measured. Inhibitory growth of compounds was reported as mean percentage of viable cells after 48 and 72 h of incubation.

4.4.3. Western blot

HCC-derived cell lines were assayed with anti-AKT, anti-phospho-AKT (Ser-473), anti-phospho-S6 Ribosomal Protein (Ser-240/244), anti-phospho-GSK-3β (Ser-9), anti-phospho-MDM2 (Ser-166), ant-phospho ERK1/2 (Cell Signalling, Danvers, MA), anti-p27 (clone 57, BD Biosciences, Franklin Lakes, NJ), anti-p53 (clone DO-7, Dakocytomation, England, UK), anti-cyclin D1 (clone DCS-6, Novocastra, Newcastle upon Tyne, UK) anti-p21 (clone F-5), anti-MDM2 (clone N-20),anti-β-catenin (clone E-5) and anti-β-actin (Santa Cruz Biotecnology, Santa Cruz, CA) antibodies. Digital images were acquired and quantified with Fluor-S MultiImager (Quantity-one,Bio-R Hercules, CA), as previously reported [31].

4.4.4. Flow cytometry analysis

For flow cytometric analysis of DNA content, 2.5×10^4 SNU449 cells in exponential growth were treated at different concentrations of the tested compounds for 48 and 72 h. After this incubation time, cells were fixed with ice-cold ethanol (70%) for 16 h at −20 °C, and treated as previously described [32] and analysed by using the FACSAria cell sorter (BD Biosciences). Detection of apoptotic cells was performed following 72 h of treatment by using Annexin V/Propidium Iodide detection kit (Bender MedSystems, Vienna, Austria) according to the manufacturer's instructions and then analysed by flow cytometry.

References

[1] J. Bruix, M. Sherman, Gastroenterology 129 (2005) 1364.
[2] A.L. Cheng, Y.K. Kang, Z. Chen, C.J. Tsao, S. Qin, J.S. Kim, R. Luo, J. Feng, S. Ye, T.S. Yang, J. Xu, Y. Sun, H. Liang, J. Liu, J. Wang, W.Y. Tak, H. Pan, K. Burock, J. Zou, D. Voliotis, Z. Guan, Lancet Oncol. 10 (2009) 25–34.
[3] K.F. Chen, H.L. Chen, W.T. Tai, W.C. Feng, C.H. Hsu, P.J. Chen, A.L. Cheng, J. Pharmacol. Exp. Ther. 337 (2011) 155–161.
[4] P. Laurent-Puig, J. Zucman-Rossi, Oncogene 25 (2006) 3778–3786.
[5] P. Laurent-Puig, P. Legoix, O. Bluteau, J. Belghiti, D. Franco, F. Binot, G. Monges, G. Thomas, P. Bioulac-Sage, J. Zucman-Rossi, Gastroenterology 120 (2001) 1763–1773.
[6] A. Villanueva, D.Y. Chiang, P. Newell, J. Peix, S. Thung, C. Alsinet, V. Tovar, S. Roayaie, B. Minguez, M. Sole, C. Battiston, S. Van Laarhoven, M.I. Fiel, A. Di Feo, Y. Hoshida, S. Yea, S. Toffanin, A. Ramos, J.A. Martignetti, V. Mazzaferro, J. Bruix, S. Waxman, M. Schwartz, M. Meyerson, S.L. Friedman, J.M. Llovet, Gastroenterology 135 (2008) 1972–1983 1983 and 1–11.
[7] K. Nakanishi, M. Sakamoto, S. Yamasaki, S. Todo, S. Hirohashi, Cancer 103 (2005) 307–312.
[8] L. Zhou, Y. Huang, J. Li, Z. Wang, Med. Oncol. (2009).

[9] S. Boyault, D.S. Rickman, A. de Reynies, C. Balabaud, S. Rebouissou, E. Jeannot, A. Herault, J. Saric, J. Belghiti, D. Franco, P. Bioulac-Sage, P. Laurent-Puig, J. Zucman-Rossi, Hepatology 45 (2007) 42–52.
[10] F. Sahin, R. Kannangai, O. Adegbola, J. Wang, G. Su, M. Torbenson, Clin. Cancer Res. 10 (2004) 8421–8425.
[11] L.V. Peng-Cheng, L. Huan-Qiu, J. Sun, Y. Zhou, H.L. Zhu, Bioorg. Med. Chem. 18 (2010) 4606–4614.
[12] Y. Dai, K. Hartandi, Z. Ji, A.A. Ahmed, D.H. Albert, L. Arnold, S.S. Arries, T. Barlozzari, J.L. Bauch, J.J. Bouska, P.F. Bousquet, G.A. Cunha, K.B. Glaser, J. Guo, J. Li, P.A. Marcotte, K.C. Marsh, M.D. Moskey, L.J. Pease, K.D. Stewart, V.S. Stoll, P. Tapang, N. Wishart, S.K. Davidsen, M.R. Michaelides, J. Med. Chem. 50 (2007) 1584–1597.
[13] B.P. Bandgar, J.V. Totre, S.S. Gawande, C.N. Khobragade, S.C. Warangkar, P.D. Kadam, Bioorg. Med. Chem. 18 (2010) 6149–6155.
[14] M.E. Prime, S.M. Courtney, F.A. Brookfield, R.W. Marston, V. Walker, J. Warne, A.E. Boyd, N.A. Kairies, W. von der Saal, A. Limberg, G. Georges, R.A. Engh, B. Goller, P. Rueger, M. Rueth, J. Med. Chem. 54 (2011) 312–319.
[15] A. Padwa, W.H. Pearson (Eds.), Synthetic Applications of 1,3-Dipolar Cycloaddition Chemistry Toward Heterocycles and Natural Products, John Wiley, New Jersey, 2003.
[16] (a) J. Elguero, in: R.A. Katritaky, C.W. Rees, E.F. Scriven (Eds.), Comprehensive Heterocyclic Chemistry II, 3, Pergamon, Oxford, 1996;
(b) L.C. Behr, R. Fusco, C.H. Jarboe, in: R.H. Wiley (Ed.), Pyrazoles, Pyrazolines, Pyrazolidines, Indazoles and Condensed Rings, Interscience Publishers, New York, 1967.
[17] T. Sakamoto, Y. Kikugawa, Chem. Pharm. Bull. 36 (1988) 800–808.
[18] S. Fustero, R. Roman, J.F. Sanz-Cervera, A. Simon-Fuentes, A.C. Cuñat, S. Villanova, M. Murguıa, J. Org. Chem. 73 (2008) 3523–3529.
[19] H.L. Liu, H.F. Jiang, M. Zhang, W.J. Yao, Q.H. Zhu, Z. Tang, Tetrahedron Lett. 49 (2008) 3805–3809.
[20] G.J. Withbroe, R.A. Singer, J.E. Sieser, Org. Process Rev. Dev. 12 (2008) 480–489.
[21] (a) G.W. Gribble, in: A. Padwa, W.H. Pearson (Eds.), Synthetic Applications of 1,3-Dipolar Cycloaddition Toward Heterocycles and Natural Products, John Wiley & Sons, New York, 2002, pp. 681–755;
(b) A. Padwa, 1,3-Dipolar Cycloaddition Chemistry, vol I, John Wiley & Sons, New York, 1984;
(c) X. Qi, J.M. Ready, Angew. Chem. Int. Ed. 46 (2007) 3242–3244;
(d) N. Jiang, C.-J. Li, Chem. Commun. (2004) 394–395;
(e) D. Vuluga, J. Legros, B. Crousse, D. Bonnet-Delpon, Green Chem. 11 (2009) 156–159.
[22] (a) B.F. Bonini, F. Boschi, M. Comes Franchini, M. Fochi, F. Fini, A. Mazzanti, A.M. Ricci, Synlett (2006) 543–547;
(b) L. Bernardi, B.F. Bonini, M. Comes Franchini, M. Fochi, M. Folegatti, S. Grilli, A. Mazzanti, A. Ricci, Tetrahedron: Asymmetry 15 (2004) 245–250.
[23] B.F. Bonini, C.M. Camaggi, M. Comes Franchini, D. Gentili, A. Pession, M. Rani, E. Strocchi, E. J. Med. Chem. 45 (2010) 2024–2033.
[24] (a) B.F. Bonini, M. Comes Franchini, D. Gentili, E. Locatelli, A.M. Ricci, Synlett (2009) 2328–2332;
(b) J. Zumbar Chandanshive, B.F. Bonini, D. Gentili, M. Fochi, L. Bernardi, M. Comes Franchini, Eur. J. Org. Chem. 33 (2010) 6440–6447;
(c) J.Z. Chandanshive, B.F. Bonini, W. Tiznado, C.A. Escobar, J. Caballero, C. Femoni, M. Fochi, M. Comes Franchini, Eur. J. Org. Chem 34 (2011) 4806–4813.
[25] G.M. Morris, D.S. Goodsell, R.S. Halliday, R. Huey, W.E. Hart, R.K. Belew, A. Olson, J. Comput. Chem. 19 (1998) 1639–1662.
[26] K.M. Nicholson, N.G. Anderson, Cell Signal. 14 (2002) 381–395.
[27] Y.S. Jung, Y. Qian, X. Chen, Cell Signal. 22 (2010) 1003–1012.
[28] M.J.S. Dewar, E.G. Zoebisch, E.F. Healy, J.J.P. Stewart, J. Am. Chem. Soc. 107 (1985) 3902–3909.
[29] M.J. Frisch, G.W. Trucks, H.B. Schlegel, G.E. Scuseria, M.A. Robb, J.R. Cheeseman, J.A. Montgomery Jr., T. Vreven, K.N. Kudin, J.C. Burant, J.M. Millam, S.S. Iyengar, J. Tomasi, V. Barone, B. Mennucci, M. Cossi, G. Scalmani, N.G.A. Rega, H. Petersson, M. Nakatsuji, M. Hada, K. Ehara, R. Toyota, J. Fukuda, M. Hasegawa, T. Ishida, Y. Nakajima, O. Honda, H. Kitao, M. Nakai, X. Klene, J.E. Li, H.P. Knox, J.B.V. Hratchian, C. CrossBakken, J. Adamo, R. Jaramillo, R.E. Gomperts, O. Stratmann, A.J. Yazyev, R. Austin, C. Cammi, J.W. Pomelli, P.Y. Ochterski, K. Ayala, G.A. Morokuma, P. Voth, J.J. Salvador, V.G. Dannenberg, S. Zakrzewski, A.D. Dapprich, M.C. Daniels, O. Strain, D.K. Farkas, A.D. Malick, K. Rabuck, J.B. Raghavachari, J.V. Foresman, Q. Ortiz, A.G. Cui, S. Baboul, J. Clifford, B.B. Cioslowski, G. Stefanov, A. Liu, P. Liashenko, I. Piskorz, R.L. Komaromi, D.J. Martin, T. Fox, M.A. Keith, C.Y. Al-Laham, A. Peng, M. Nanayakkara, P.M.W. Challacombe, B. Johnson Gill, W. Chen, M.W. Wong, C. Gonzalez, J.A. Pople, Gaussian 03, Gaussian, Inc., Wallingford, CT, 2004.
[30] H.M. Shapiro, Practical Flow Cytometry, second ed. John Wiley & Sons, New York, 1988, p. 129.
[31] L. Gramantieri, M. Ferracin, F. Fornari, A. Veronese, S. Sabbioni, C.G. Liu, G.A. Calin, C. Giovannini, E. Ferrazzi, G.L. Grazi, C.M. Croce, L. Bolondi, M. Negrini, Cancer Res. 67 (2007) 6092–6099.
[32] F. Fornari, L. Gramantieri, M. Ferracin, A. Veronese, S. Sabbioni, G.A. Calin, G.L. Grazi, C. Giovannini, C.M. Croce, L. Bolondi, M. Negrini, Oncogene 27 (2008) 5651–5661.